Numerical Results and Discussion

Figure 1 shows the results obtained from the first-order formula, Eq. (9), for a single-degree-of-freedom linear oscillator under Gaussian white noise excitation and for rather low safety threshold levels $\pm 2\sigma$, where σ is the standard deviation of the stationary response. The Poisson and the nonapproaching excursion estimates are also plotted for comparison. Within the time range investigated, Eq. (9) gives a higher estimate than the corresponding Poisson and nonapproaching excursion estimates.

Figure 2 shows the results obtained from the second-order formula, Eq. (16), in the time region where the asymptotic form Eq. (20) for $E[\eta^2(t)]$ is applicable and for relatively high safety bounds $\pm 3.50\sigma$. Corresponding results computed from Eq. (9) are also plotted for comparison. The comparison reveals that using the most uncertain $\eta(t)$ as a criterion, a first-order estimate may not always be more conservative than a second-order estimate.

Another point of interest is that all the second-order estimates tend to straight lines when plotted on a semilogarithmic scale. This implies that these estimates tend to the exponential form, a general form conjectured by Mark[5] and verified by Crandall, et al.[2] by simulation. For example, for damping ratio $\zeta = 0.02$ and failure bounds $\pm 3.5\sigma$ the second order estimate of $P_0(t)$ tends to $\exp(-0.00279$ natural cycles), suggesting an average first excursion time in the neighborhood of $1/0.00279 = 357$ natural cycles. The simulation results[2] for the same system have an average of 744 cycles.

Equations (9) and (16) were obtained from maximization of the entropy of $\eta(t)$. A different estimate for P_0 would result if maximization was associated with a random variable other than $\eta(t)$. Tribus[4] has shown that the maximum entropy estimate for P_0 with the knowledge of the average structural life, L, is given by

$$P_0(t) = \exp(-t/L) \tag{21}$$

However, no general method is available to compute L for a practical structural response. Note that Eq. (21) would agree with the Poisson estimate if L could be replaced by $1/g_1$. Clearly, $1/g_1$ is the average recurrence time which is a conditional average whereas L is an unconditional average. From a physical argument we can assert that $L \leq 1/g_1$. If, however, we are ignorant of any statistical relationship between different excursions, then the assumption of independent excursions should be the most unbiased one, and Eq. (21) would coincide with the Poisson estimate.

It is appropriate to comment on the general philosophy of a statistical analysis from the standpoint of maximum uncertainty. Since nearly all experimental measurements of a random phenomenon are directed toward the first- and the second-order moments, our knowledge of the physical situation is seldom beyond these levels. However, when theoretical computation requires an expression for the probability distribution, an analyst is forced to extrapolate from his limited knowledge. Such extrapolations are sometimes dictated by mathematical conveniences. Thus, the Gaussian distribution is often a favorite assumption because of its desirable mathematical properties. For example, a Gaussian structural response has been assumed in the computation of $g_1(t)$ and $f_2(t_1,t_2)$ reported herein. This procedure is quite justified, however, since the Gaussian random process is associated with the maximum entropy if our knowledge of the response is limited to the mean and the correlation functions. To estimate the structural reliability from the functions $g_1(t)$ and $f_2(t_1,t_2)$, we used, once again, the maximum entropy principle and arrived at Eqs. (9) and (16). Thus, Eqs. (9) and (16) were the results of repeated applications of the maximum entropy principle. These are the least prejudiced estimates subject to the respective constraints of statistical knowledge. The maximum entropy results are also expected to be conservative as supported by one example where the estimated average structural life is about one-half the simulation average.

Finally, it should be noted that although a single-degree-of-freedom system was chosen in the example, the present method applies to any structure as long as the functions $g_1(t)$ and $f_2(t_1,t_2)$ can be calculated.

References

[1] Lin, Y. K., "First-Excursion Failure of Randomly Excited Structures," *AIAA Journal*, Vol. 8, No. 4, April 1970, pp. 720–725.

[2] Crandall, S. H., Chandiramani, K. L., and Cook, R. G., "Some First Passage Problems in Random Vibration," *Journal of Applied Mechanics*, Vol. 33, No. 3, 1966, pp. 532–538.

[3] Jaynes, E. T., "New Engineering Applications of Information Theory," *Proceedings of the First Symposium on Engineering Applications of Random Function Theory and Probability*, edited by J. L. Bogdanoff and F. Kozin, Wiley, New York, 1963, pp. 163–203.

[4] Tribus, M., "The Use of the Maximum Entropy Estimate in the Estimation of Reliability," *Recent Development in Information and Decision Processes*, edited by R. E. Machol and P. Gray, Macmillan, New York, 1962, pp. 102–140.

[5] Mark, W. D., "On False-Alarm Probabilities of Filtered Noise," *Proceedings of the IEEE*, Vol. 54, No. 2, 1966, pp. 316–317.

Flow with $M_\infty = 1$ Past Thin Airfoils

JOHN R. SPREITER*
Stanford University, Stanford, Calif.

AND

STEPHEN S. STAHARA†
Nielsen Engineering & Research Inc., Mountain View, Calif.

IT has been recognized for some time that the pressure distribution on thin nonlifting airfoils in steady two-dimensional flow with freestream Mach number M_∞ equal to, or near, unity may be calculated by means of the local linearization theory.[1-3] The purpose of this note is threefold: 1) to present some alternative, but equivalent, expressions for the pressure that are more convenient for numerical computation than those given heretofore, 2) to present results for the airfoils tested by Michel et al.[4,5] using the exact equations to describe the airfoil ordinates rather than close approximations which permit analytical solutions as done originally, and 3) to examine the discrepancies that appear near the trailing edge in nearly all comparisons of theoretical and experimental pressure distributions for $M_\infty = 1$ to determine whether they may be inherent in the inviscid flow, as opposed to the usual explanation that they are due to shock-wave boundary-layer interaction.

According to the local linearization theory, the pressure coefficient C_p, or its transonic similarity counterpart $\bar{C}_p = [M_\infty^2(\gamma+1)/\tau^2]^{1/3}C_p$, at an arbitrary point x on the surface of a thin nonlifting airfoil having ordinates Z and thickness-chord ratio $\tau = t/c$ in a flow with $M_\infty = 1$ and ratio of specific heats γ (for air, $\gamma = \frac{7}{5}$) is given by

$$\bar{C}_p = -2\left\{\frac{3}{\pi}\int_{x^*}^{x}\left[\frac{d}{dx_1}\int_0^{x_1}\frac{d(Z/\tau)/d\xi}{(x_1-\xi)^{1/2}}\,d\xi\right]^2 dx_1\right\}^{1/3} = -2\left\{\frac{3}{\pi}\int_{x^*}^{x}[F(x_1)]^2\,dx_1\right\}^{1/3} \tag{1}$$

Received May 4, 1970. This work was supported by NASA Ames Research Center under Contract NAS2-5410.

* Professor, Departments of Applied Mechanics and Aeronautics and Astronautics; Consultant, Nielsen Engineering & Research, Inc. Associate Fellow AIAA.

† Senior Research Scientist. Member AIAA.

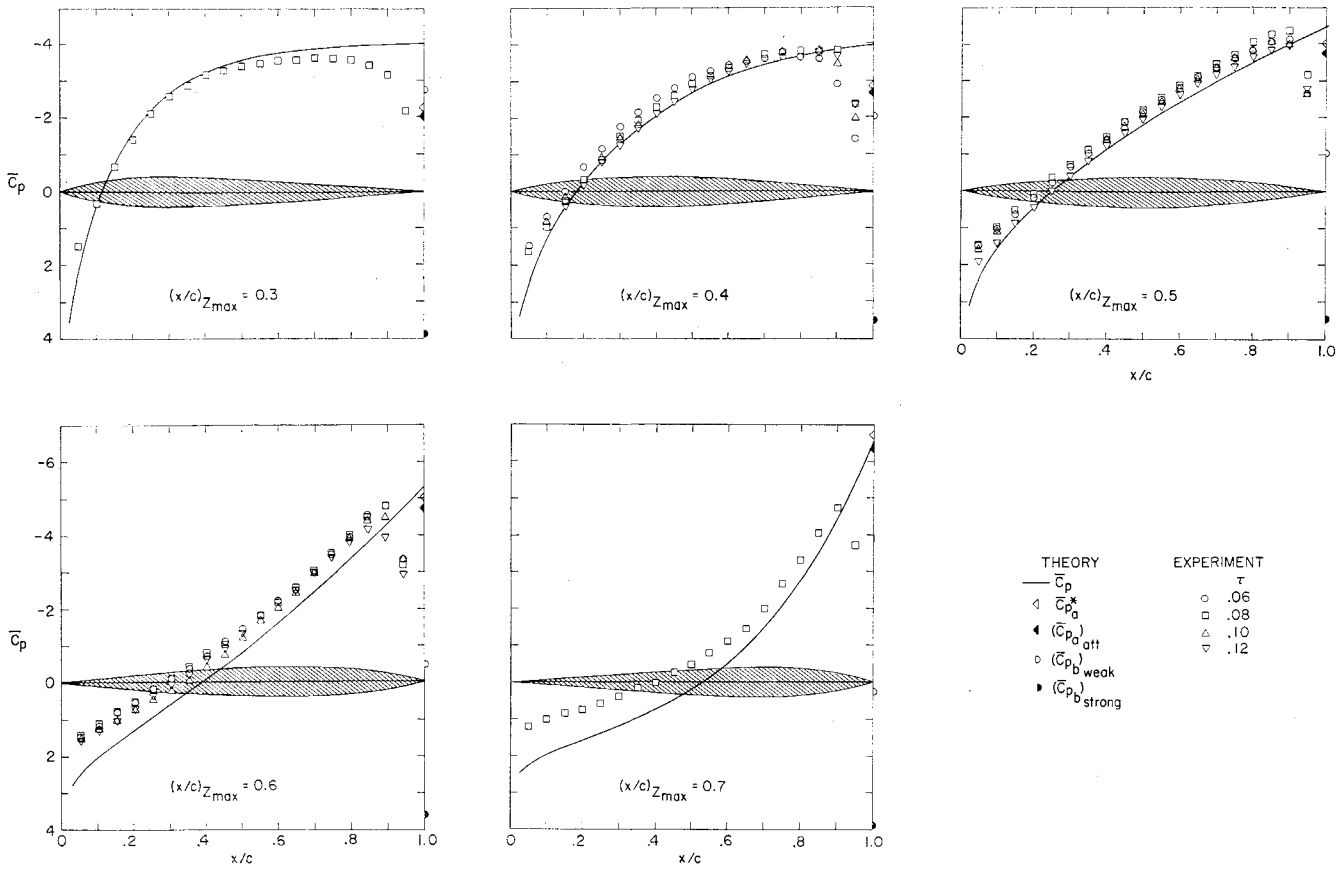

Fig. 1 Theoretical and experimental[4,5] pressure distributions for several airfoils having various thickness-chord ratios τ and locations $(x/c)_{Z_{max}}$ of the point of maximum thickness.

where x^* represents the location of the sonic point. For smoothly curving airfoils, x^* is equal to the value for x_1 at which the function $F(x_1)$ vanishes. Equation (1) is concise and convenient for application to airfoils having ordinates given by analytic expressions such as those considered in the original references. Even for those airfoils, however, it was necessary to approximate some of the airfoil shapes so that Eq. (1) could be integrated analytically. An alternate procedure that can be applied to these airfoils, and many others as well, would be to perform the integrations numerically. It this is done, however, the square root singularity of the integrand at $x_1 = \xi$ makes it inconvenient for numerical computation. Three alternative expressions for $F(x_1)$ that can be derived by straightforward operations of integration by parts, differentiation, and addition and subtraction of equal quantities are

$$F(x_1) = \frac{Z'(x_1)}{\tau}\frac{1}{(x_1)^{1/2}} + \frac{2Z''(x_1)}{\tau}(x_1)^{1/2} + \frac{d}{dx_1}\int_0^{x_1}\frac{Z'(\xi)-Z'(x_1)}{\tau(x_1-\xi)^{1/2}}\,d\xi$$

$$= \frac{Z'(0)}{\tau}\frac{1}{(x_1)^{1/2}} + \frac{d}{dx_1}\int_0^{x_1}\frac{2Z''(\xi)}{\tau}(x_1-\xi)^{1/2}d\xi$$

$$= \frac{Z'(0)}{\tau}\frac{1}{(x_1)^{1/2}} + \frac{2Z''(0)}{\tau}(x_1)^{1/2} + 2\int_0^{x_1}\frac{Z'''(\xi)}{\tau}(x_1-\xi)^{1/2}d\xi \quad (2)$$

where the primes indicate differentiation in the usual manner, and the indicated arguments of the quantities signify where, or in terms of which variable, they are to be evaluated; i.e., $Z'(\xi)$ signifies $dZ/d\xi$ with Z expressed as a function of ξ, and $Z'(0)$ signifies dZ/dx evaluated at $x = 0$, etc.

Because of the prior existence of experimental data, a family of airfoils was considered in Ref. 1 that had ordinates Z and chordwise location $(x/c)_{Z_{max}}$ of the maximum thickness

$$Z/c = A[x/c - (x/c)^n],\ (x/c)_{Z_{max}} = (1/n)^{1/(n-1)} \quad (3)$$

and

$$Z/c = A[1 - x/c - (1 - x/c)^n],\ (x/c)_{Z_{max}} = 1 - (1/n)^{1/(n-1)} \quad (4)$$

in which $A = [\tau n^{n/(n-1)}]/[2(n-1)]$. Values for n of 2, 3.38, and 6.05 were chosen by the experimenters so that $(x/c)_{Z_{max}}$ of the airfoils defined by Eq. (3) were 0.50, 0.60, and 0.70; and that of the airfoils defined by Eq. (4) were 0.50, 0.40, and 0.30. To facilitate analytic integration, the ordinates of the airfoils described by Eq. (4) were approximated in Ref. 1 by replacing $n = 3.38$ by 3 and 3.5, and $n = 6.05$ by 6.

We now adopt the alternative procedure of retaining the exact expressions for the airfoil ordinates, but performing the integrations numerically using the expressions of Eq. (2) for $F(x_1)$. Pressure distributions calculated in this way for the five families of airfoils described previously are shown in Fig. 1 together with experimental data[4,5] for several airfoils having $\tau = 0.06$, 0.08, 0.10, and 0.12. As indicated more briefly recently,[6] the results for $n = 3.38$ are intermediate between those for $n = 3.0$ and 3.5, as they should be. The new results for $n = 6.05$ are virtually indistinguishable from the previous theoretical results for $n = 6$. Except for the immediate vicinity of the trailing edge, these comparisons indicate essential agreement between the calculated and measured pressure distributions. The general trend of the theory to agree better with the data for thicker airfoils and for airfoils with maximum thickness forward has been examined in some detail previously,[7] and found to be consistent with the antici-

Table 1 Significant values for $\bar{C}_p$ and slope at the trailing edge of the airfoils presented in Fig. 1

$(x/c)_{Z_{max}}$	0.30	0.40	0.50	0.60	0.70
$[d(Z/\tau)/dx]_a$	−0.86	−1.18	−2.00	−2.82	−4.32
$\bar{C}_{p_a}$	−4.04	−3.96	−4.45	−5.23	−6.61
$(\bar{C}_{p_a})_{att}$	−2.15	−2.67	−3.78	−4.75	−6.32
$\bar{C}_{p_a}{}^*$	−2.27	−2.82	−4.00	−5.03	−6.68
$(\bar{C}_{p_b})_{weak}$	−2.73	−2.03	−1.04	−0.53	0.25
$(\bar{C}_{p_b})_{strong}$	3.86	3.57	3.42	3.60	3.91

pated effects of wind-tunnel wall interference and of the viscous boundary layer.

With respect to the differences that occur near the trailing edge, the question arises whether they are primarily the result of boundary-layer shock-wave interaction, as most would suppose, or whether they might be inherent in the inviscid solution. The latter would be the case if the local Mach number immediately upstream of the trailing edge were not high enough for an oblique shock wave to turn the flow through the required angle. If that should occur, the shock wave would detach from the trailing edge and move forward onto the aft part of the airfoil, substantially altering the pressure distribution there.

To investigate this possibility, we must consider the following expression[8] for the transonic approximation for the shock polar, where u and w refer to the Cartesian components of the perturbation velocity and subscripts a and b refer to conditions ahead and behind the shock wave:

$$(1 - M_\infty{}^2)(u_a - u_b)^2 + (w_a - w_b)^2 = \frac{M_\infty{}^2(\gamma + 1)}{U_\infty}\left(\frac{u_a + u_b}{2}\right)(u_a - u_b)^2 \quad (5)$$

Upon introducing $C_p = -2u/U_\infty$ and $dZ/dx = w/U_\infty$, where U_∞ refers to the free-stream velocity, and setting $M_\infty = 1$, $(dZ/dx)_b = 0$, and expressing the relations in terms of $\bar{C}_p$ rather than C_p, Eq. (5) becomes

$$[d(Z/\tau)/dx]_a{}^2 = -\tfrac{1}{16}(\bar{C}_{p_a} + \bar{C}_{p_b})(\bar{C}_{p_b} - \bar{C}_{p_a})^2 \quad (6)$$

With $[d(Z/\tau)/dx]_a$ known from the geometry of the airfoil, and $\bar{C}_{p_a}$ to be as indicated by the local linearization theory, this relation may be solved for $\bar{C}_{p_b}$, the reduced pressure coefficient immediately downstream of the trailing edge, provided $-\bar{C}_{p_a}$ is sufficiently large for the shock wave to be attached to the trailing edge. If $-\bar{C}_{p_a}$ is less than a limiting value $(-\bar{C}_{p_a})_{att}$, which depends on $[d(Z/\tau)/dx]_a$, it is not possible for an oblique shock wave to turn the flow the required angle. The appropriate expression for $(-\bar{C}_{p_a})_{att}$ may be determined by solving

$$\frac{d}{d\bar{C}_{p_b}}\left[\frac{d(Z/\tau)}{dx}\right]_a^2 = -\frac{1}{16}(\bar{C}_{p_b} - \bar{C}_{p_a})(3\bar{C}_{p_b} + \bar{C}_{p_a}) = 0 \quad (7)$$

for $\bar{C}_{p_b}$ in terms of $\bar{C}_{p_a}$ to obtain $\bar{C}_{p_b} = -\bar{C}_{p_a}/3$, and substituting into Eq. (6) to obtain

$$(\bar{C}_{p_a})_{att} = -(3/2^{1/3})[d(Z/\tau)/dx]_a{}^{2/3} \quad (8)$$

A necessary condition for the shock wave to be attached to the trailing edge of the airfoil is thus that $\bar{C}_{p_a} \leq (\bar{C}_{p_a})_{att}$. It may be seen from the values listed for $\bar{C}_{p_a}$ and $(\bar{C}_{p_a})_{att}$ in Table 1 that this condition is satisfied for each of the airfoils for which results are shown in Fig. 1.

The margin by which this condition is exceeded diminishes rapidly as the maximum thickness moves aft on the airfoil, however, and it seems likely that the condition for an attached shock wave may not be satisfied for airfoils of this family if the maximum thickness were much further aft than the most extreme of the cases considered, namely 0.70 chord.

A further condition required for the surface pressure distribution to be independent of conditions downstream of the airfoil in the absence of a boundary layer is that the flow be supersonic downstream of the trailing shock wave. Now, it is a well-known property of the transonic shock polar that can be seen from Eq. (6), or the listings of Table 1, that $\bar{C}_{p_b}$ may be either positive or negative, but that $\bar{C}_{p_a} < \bar{C}_{p_b} \leq -\bar{C}_{p_a}$ if attention is confined to physically significant compressive shock waves described by real solutions of Eq. (6). Of the two solutions of that equation that satisfy this condition, one is always positive, indicating subsonic flow, and the other may be positive or negative, indicating either subsonic or supersonic flow. To illustrate this point further, the two values for $\bar{C}_{p_b}$ are indicated by solid and open half circles for each of the airfoils on Fig. 1. The limiting value for $\bar{C}_{p_a}$ for which the flow is exactly sonic immediately downstream of a shock wave attached to the trailing edge is designated by $\bar{C}_{p_a}{}^*$ and may be determined from Eq. (6) by setting $\bar{C}_{p_b}$ equal to zero. It is

$$\bar{C}_{p_a}{}^* = -2^{4/3}[d(Z/\tau)/dx]_a{}^{2/3} \quad (9)$$

Values for $\bar{C}_{p_a}{}^*$ are listed in Table 1 for each of the airfoils for which results are shown in Fig. 1.

If $\bar{C}_{p_a}{}^* \leq \bar{C}_{p_a} \leq (\bar{C}_{p_a})_{att}$, a shock wave may be attached to the trailing edge, but the flow immediately downstream of it must be subsonic. Under these circumstances, which prevail for the airfoils of Fig. 1 with maximum thickness at 0.70 chord, effects arising in the wake and elsewhere downstream of the airfoil inevitably influence conditions at the trailing edge. This result opens the possibility that these influences might be sufficient, under certain circumstances, to cause the trailing shock wave to move forward onto the airfoil, and thereby to produce at least part of the discrepancies apparent in Fig. 1 between the theoretical and experimental pressure distributions near the trailing edge.

If $\bar{C}_{p_a} < \bar{C}_{p_a}{}^* < (\bar{C}_{p_a})_{att}$, as it is for the remainder of the airfoils considered in Fig. 1, the shock wave may be attached to the trailing edge, but the flow immediately downstream of it may be either subsonic or supersonic according to whether the shock wave is strong or weak. If the shock wave is of the strong type, the situation would be substantially the same as just described; and the sources of the differences between the theoretical and experimental pressure distributions near the trailing edge might be sought in either inviscid or viscous phenomena. If, on the other hand, the shock wave is of the weak type, the flow is supersonic immediately downstream of the shock wave, and no effects of downstream origin can influence conditions at the airfoil in the absence of viscosity. To the extent that this prevails, the preceding results support the general belief that the differences between theoretical and experimental pressure distributions over the aft portion of airfoils with small or moderate trailing-edge angles must involve viscous processes, in particular, effects of shock-wave boundary-layer interaction. While the inviscid theory is capable of providing a good approximation for the pressure distribution over most of the airfoil, the nature and magnitude of the deficiencies near the trailing edge indicate that an improved theory, which includes viscous effects, is required to provide satisfactory predictions of drag at $M_\infty = 1$.

References

[1] Spreiter, J. R. and Alksne, A. Y., "Thin Airfoil Theory Based on Approximate Solution of the Transonic Flow Equation," Rept. 1359, 1958, NACA (supersedes TN 3970, NACA).

[2] Spreiter, J. R., "Aerodynamics of Wings and Bodies at Transonic Speeds," *Journal of the Aerospace Sciences*, Vol. 26, No. 8, Aug. 1959, pp. 465–487.

[3] Spreiter, J. R., "The Local Linearization Method in Transonic Flow Theory," *Symposium Transsonicum*, edited by K. Oswatitsch, Springer-Verlag, Berlin/Göttingen/Heidelberg, 1964, pp. 152–183.

[4] Michel, R., Marchaud, F., and Le Gallo, J., "Étude des écoulements transsoniques autour des profils lenticulaires, a incidence nulle," Pub. 65, 1953, ONERA.

[5] Michel, R., Marchaud, F., and Le Gallo, J., "Influence de la position du maitre-couple sur les écoulements transsoniques autour de profils a pointes," Pub. 72, 1954, ONERA.

[6] Spreiter, J. R. and Stahara, S. S., "Developments in Transonic Flow Theory," *Zeitschrift für Flugwiss* 18, Heft 2/3, 1970, pp. 33–40.

[7] Spreiter, J. R., Alksne, A. Y., and Hyett, B. J., "Theoretical Pressure Distributions for Several Related Nonlifting Airfoils at High Subsonic Speeds," TN 4148, 1958, NACA.

[8] Spreiter, J. R., "On the Application of Transonic Similarity Rules to Wings of Finite Span," Rept. 1153, 1953, NACA (supersedes NACA TN 2726).

Determination of Axial Gradient Effects in Freejet Flows

A. G. Keel Jr.* and R. N. Zapata†
University of Virginia, Charlottesville, Va.

Nomenclature

$C_{D\text{nose}}$ = value of drag coefficient based on parameters at model nose
d_0 = nominal diameter of source orifice
D = model base diameter
$Kn_{ri}(r_n)$ = λ_{ri}/r_n
L = model length
M_{is} = isentropic axial Mach number
$Re_{w,L}$ = $\rho_\infty U_\infty L/\mu_w$, where μ_w is viscosity coefficient based on T_w
r_n, r_B = radius of model nose, radius of model base
T_w = model wall temperature
U_∞ = freestream (axial) velocity
$\langle v_r \rangle$ = $2(2RT_w/\pi)^{1/2}$, mean thermal speed of reflected molecules
λ_∞ = hard sphere mean-free-path of incident molecules
ρ_{fip} = freestream value of incident stream density at first interaction point of reflected with incident molecule
ρ_{nose} = freestream value of incident stream density at model nose
ρ_∞ = freestream incident density
$\Delta\rho$ = axial variation in freestream density across model length
Ψ = r_n/r_B, model bluntness ratio

Introduction

In this Note an empirical technique for assessing the influence of axial flow gradients in free jets on the measurements of drag coefficients of slender, blunted cones at zero angle-of-attack is discussed. Specific results obtained for low-density flows are used to predict the values of the drag coefficient for the case of a uniform flow characterized by the flow parameters at the nose of the cones.

Experimental Method

A schematic of the experimental apparatus is shown in Fig. 1. The freejet flow is produced by allowing gas to emerge from the stagnation chamber through a thin-plate orifice into a vacuum. The conical model is supported in midstream by an electromagnetic balance. A careful calibration procedure makes it possible to relate the magnitude of the current through the supporting coils to the magnitude of the aerodynamic force with high accuracy and precision.[1] The axial jet-core flow properties are a function of the axial position scaled with respect to the (effective) source orifice diameter.[2]

Received May 5, 1970; revision received June 19, 1970. Research supported by Grant AFOSR-69-1798. The assistance of R. D. Passmore in the data acquisition and reduction is gratefully acknowledged.

* Assistant Research Engineer.
† Associate Professor. Member AIAA.

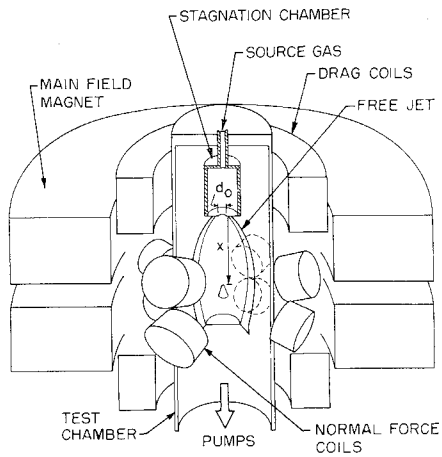

Fig. 1 Schematic of experiment.

To study the influence of flow gradients on the aerodynamic characteristics of cones, the magnitude of these gradients was varied by varying the size of the source orifice. By adjusting the axial position of the models in the freejet, the Mach number at the nose of the cones could be made the same in every case. A total of four source orifices and four models were used in this investigation (see Table 1). By varying the source pressure a range of the correlating flow parameter, $Re_{w,L}$, between 2.5 and 100 was obtained.

Results and Discussion

Results of the tests for one model are plotted in Fig. 2 (three lower traces of solid symbols) as a family of curves of C_D vs $Re_{w,L}$ for different magnitudes of the axial gradients of the freejet flow. An indication of the magnitude of the variation of the flow parameters over the length of the cones ($\Delta\rho/\rho_{\text{nose}}$) can be found in Table 1. From these and similar results obtained with other models two consistent trends emerge. First, in the higher $Re_{w,L}$ range the curves of a family are parallel and eventually become linear in the log-log plot. Second, as $Re_{w,L}$ is decreased, the curves in a family diverge, with the point of divergence occurring at a higher value of $Re_{w,L}$ when the flow gradients are steeper (i.e., the source orifice is smaller). These two trends suggest two distinct effects of flow gradients on the aerodynamics of a test body.

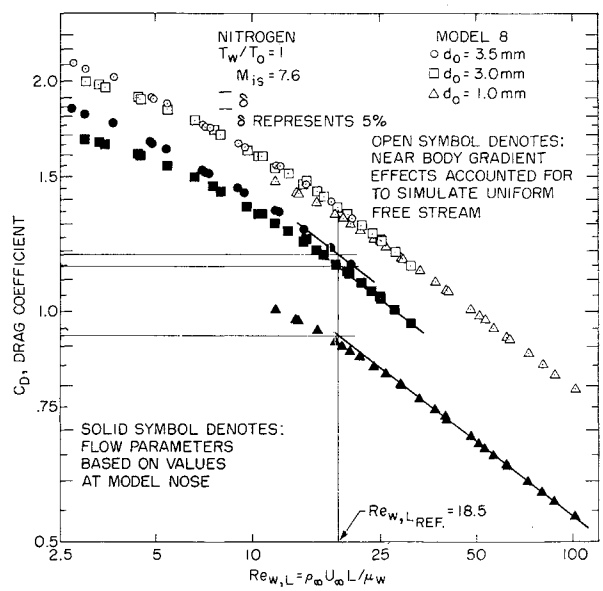

Fig. 2 C_D vs $Re_{W,L}$ for gradient flow and for corresponding uniform freestream.